Electronic Supplementary Material (ESI) for Energy & Environmental Science.
This journal is © The Royal Society of Chemistry 2023

Electronic Supplementary Material (ESI) for Energy & Environmental Science.
This journal is © The Royal Society of Chemistry 2023

Supporting Information

Ultraconformal chemo-mechanical stable cathode interface for high-performance all-solid-state batteries at wide temperatures

Zichen Zhang,[a] Wanqing Jia,[a] Yu Feng,[a] Ruopeng Ai,[a] Jialu Yu,[a] Xiaofei Bie,[b] Ximin Zhai,[b] Tao Jiang,[b] Shiyu Yao*[a] and Fei Du*[a]

Experimental Procedures

Preparation of m-NCM and s-NCM: The m-NCM is a commercial product. The s-NCM powders were obtained from m-NCM by mechanical ball milling method. The specific process was that the m-NCM powders were put into a ZrO_2 pot with ZrO_2 balls (ϕ = 5 mm, the mass ratio of balls to materials was 30:1), and then preparation process was performed using a planetary ball milling apparatus at 200 rpm for 2 h.

Preparation of the Li_3InCl_6 SE: Lithium chloride (LiCl, Aladdin, 99.0%) and indium chloride ($InCl_3$, Aladdin, 99.99%) were weighed to the stoichiometric molar ratio. The mixtures were mechanically mixed in a ZrO_2 pot with ZrO_2 balls (ϕ = 5 mm, the mass ratio of balls to mixtures was 20:1). The mixing process was performed using a planetary ball milling apparatus at 600 rpm for 24 h. And then the ball-milled powders were sealed in a glass tube at ~10 Pa under vacuum, annealed at 400 ^oC for 12 hours with a ramping rate of 5 ^oC per minute, and cooled to room temperature naturally. All the preparation processes were carried out with an Ar atmosphere.

Preparation of the Li_6PS_5Cl SE: Lithium sulfide (Li_2S, Aladdin, 99.5%), phosphorus pentasulfide (P_2S_5, Aladdin, 99.0%) and lithium chloride (LiCl, Aladdin, 99.0%) were weighed to the stoichiometric molar ratio. The mixtures were mechanically mixed in a ZrO_2 pot with ZrO_2 balls (ϕ = 5 mm, the mass ratio of balls to mixtures was 20:1). The mixing process was performed using a planetary ball milling apparatus at 400 rpm for 12 h. And then the ball-milled powders were sealed in a glass tube at ~10 Pa under vacuum, annealed at 550 ^oC for 15 hours with a ramping rate of 1.5 ^oC per minute, and

cooled to room temperature naturally. All the preparation processes were carried out in an Ar atmosphere.

Preparation of the composited cathode: For B-NCM@Li_3InCl_6, m-NCM and Li_3InCl_6 with the mass ratio at several specific ratios ranging from 60:40 to 80:20 were mechanically mixed in a ZrO_2 pot with ZrO_2 balls (ϕ = 5 mm, the mass ratio of balls to mixtures was 20:1). The mixing process was performed using a planetary ball milling apparatus at 200 rpm or 400 rpm for 2h. m-NCM@Li_3InCl_6 was obtained by hand grinding m-NCM and Li_3InCl_6 with a mass ratio of 65:35 in an agate mortar for 30 minutes. s-NCM@Li_3InCl_6 was obtained by hand grinding s-NCM and Li_3InCl_6 which had been treated using the same ball-milled conditions as B-NCM@Li_3InCl_6 with a mass ratio of 65:35 in an agate mortar for 30 minutes. All the preparation processes were carried out in an Ar atmosphere.

Preparation of Liquid-Electrolyte batteries: Liquid-Electrolyte batteries based on s-NCM, s-NCM cathode active materials were assembled as 2032-type coin cells. The cathode electrodes were fabricated by casting a slurry consisting of 80 wt% NCM active material, 10 wt% AB as the conductive additive, and 10 wt% Poly(vinylidene fluoride) (PVdF) solved in N-methylpyrrolidone (NMP) as a binder on an aluminum foil. Lithium metal was used as a counter electrode. The electrolyte solution was 1 mol L^{-1} $LiPF_6$ in ethylene carbonate (EC) and ethyl methyl carbonate (EMC) mixture (3:7 ratio by weight). All the battery assembly processes were carried out in an Ar-filled glove box.

Preparation of ASSLBs: ASSLBs were assembled in a 10 mm polyether ether ketone (PEEK) dies with two stainless steel plungers. First, SE layers were formed by pelletizing 80 mg of Li_6PS_5Cl powders. Then, the 5~6 mg as-prepared composited cathode was spread on one side of the SE layer while the counter electrode (Li-In foils, the lithium foil and indium foil with a molar ratio of 3:7 were cold-pressed at 370 MPa for 1 min) was put on the other side. Finally, the whole assemblies were pressed at 370 MPa for 1min, and then the pressure was maintained at 50 MPa for subsequent electrochemical performance tests. All the battery assembly processes were carried out in an Ar-filled glove box.

Characterizations: Powder XRD patterns were recorded by Bruker D8 Advance

diffractometer with Cu Kα radiation (λ = 1.5406 Å). The atomic ratios of samples were determined by ICP (Thermo iCAPQc) measurements. Nitrogen adsorption-desorption isotherms were recorded on a kubo X1000 instrument, and the Brunauer-Emmett-Teller (BET) model was used to calculate the specific area. XPS analysis was performed with a VG scientific ESCALAB-250 spectrometer. The morphologies and the microstructures of samples were investigated using the field-emission SEM (Hitachi Regulus8100 FESEM). The transmission electron microscopy (TEM) analysis of B-NCM@Li_3InCl_6 involved dispersing the cathode in methylene bromide. Subsequently, the resulting microwaved solution was deposited onto a microgrid copper mesh and dried in an argon-filled glovebox. The morphologies and microstructures were examined using a TEM instrument (JEM-2100F) equipped with a probe corrector operating at 200 kV. Since Li_3InCl_6 is highly sensitive to the high-energy electron beams in TEM, we employed both significantly reduced beam intensity with a current density of 21.5 pA cm^{-2} and an extremely short acquisition time of 0.2 s to minimize any potential adverse effects. FIB-SEM (SOLARIS/TESCAN) was used to observe the cross-section morphology of cathode particles in composited cathode (the operating voltage and emission current of the electron beam were 5 kV and 0.1 nA, respectively). The Vickers hardness of three composited cathodes was tested using a microhardness tester (Hv-51S) with the applied load of 200 g, and the morphology of indentation was characterized using a scanning electron microscope (SEM, FEI Magellan 400).[1] The Young's moduli of three composited cathodes were measured by AFM (Dimension Icon-XR, Bruker) in peak force quantitative nanomechanical mapping mode and analyzed by Derjaguin-Muller-Toporov model.

Electrochemical characterizations: For the measurement of ionic and electronic conductivities of Li_6PS_5Cl and Li_3InCl_6, 80 mg of Li_6PS_5Cl or Li_3InCl_6 powders were prepared in 10 mm polyether ether ketone (PEEK) dies with two stainless steel plungers followed by pressing at 375 MPa with a hydraulic press. EIS measurements were performed from 5 MHz to 1 Hz with an applied potential of 50 mV using a Solartron 1260 impedance analyzer at several specific temperatures ranging from -20 to 25 ^oC. The direct current (DC) polarizations were obtained by applying 0.8 V bias potentials for 20 min using a Bio-Logic electrochemical workstation with the same equipment at

25 °C. Galvanostatic tests of batteries were carried out by using LAND CT-3002A (Wuhan, China) automatic battery tester. Among them, for GITT analysis, the cells were cycled with the duration time for each applied galvanostatic current and rest at 15 min and 4 h, respectively. EIS data were collected using a VSP multichannel potentiostatic-galvanostatic system (Biologic, France) over a frequency range of 1 MHz to 10 mHz. All the tests for batteries were completed with the help of the thermostats.

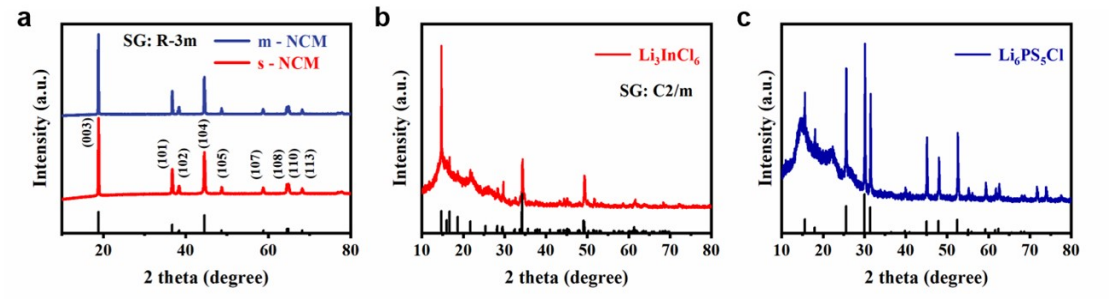

Figure S 1 XRD of pristine powders: (a) m-NCM and s-NCM, (b) Li_3InCl_6 and (c) Li_6PS_5Cl

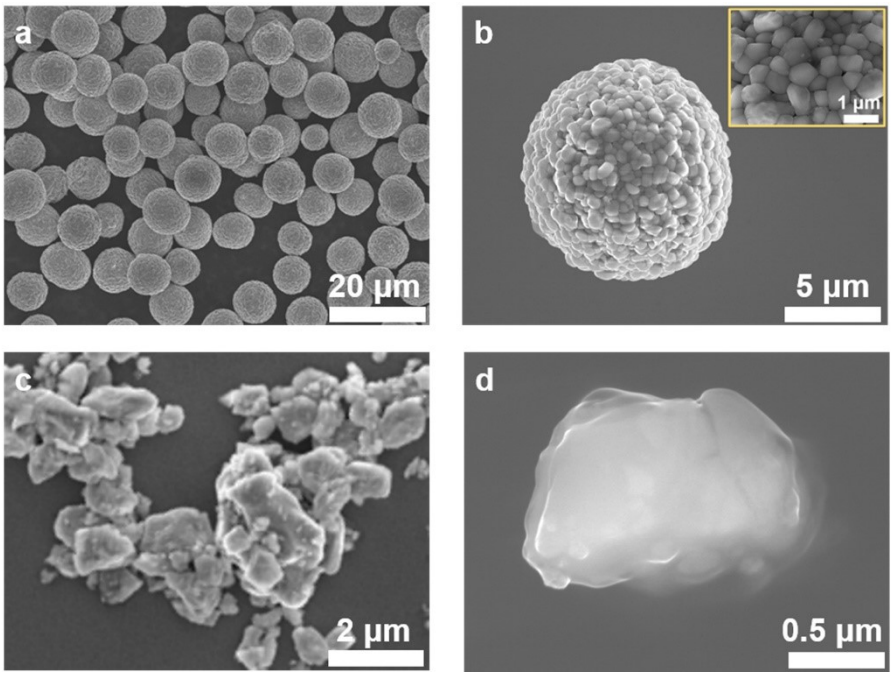

Figure S 2 SEM images of pristine powders of: (a, b) m-NCM and (c, d) s-NCM.

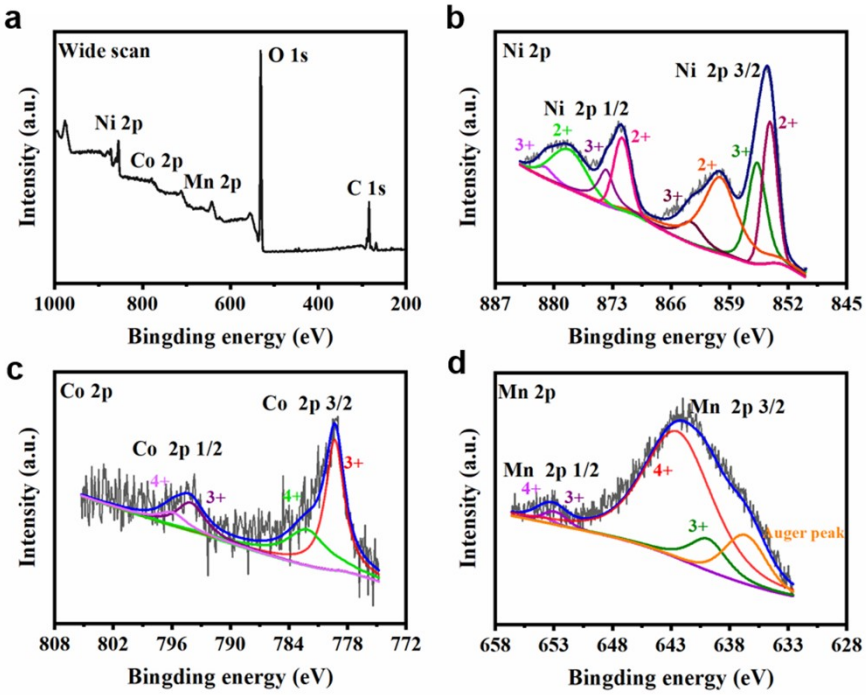

Figure S 3 XPS spectra of the m-NCM.

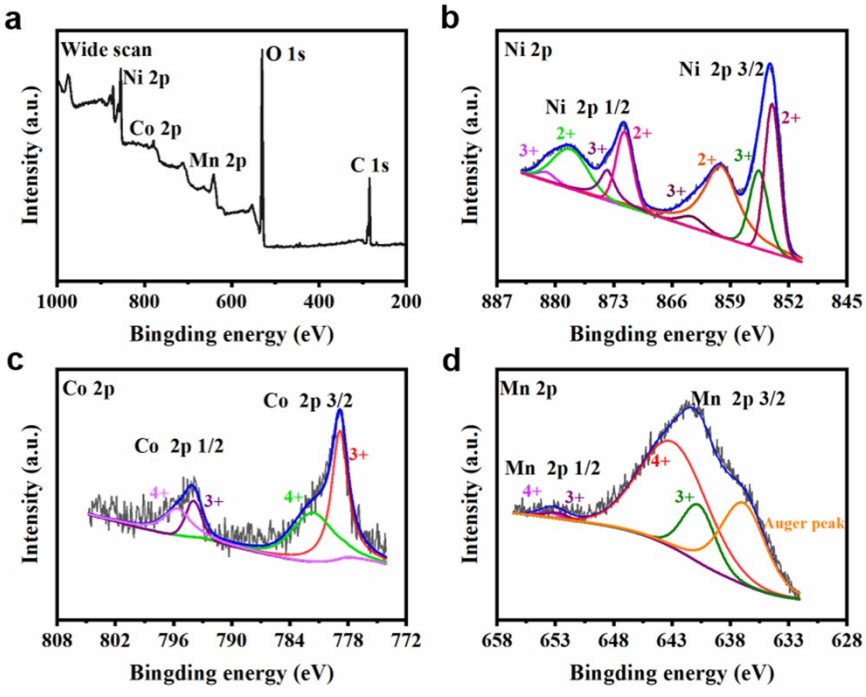

Figure S 4 XPS spectra of the s-NCM

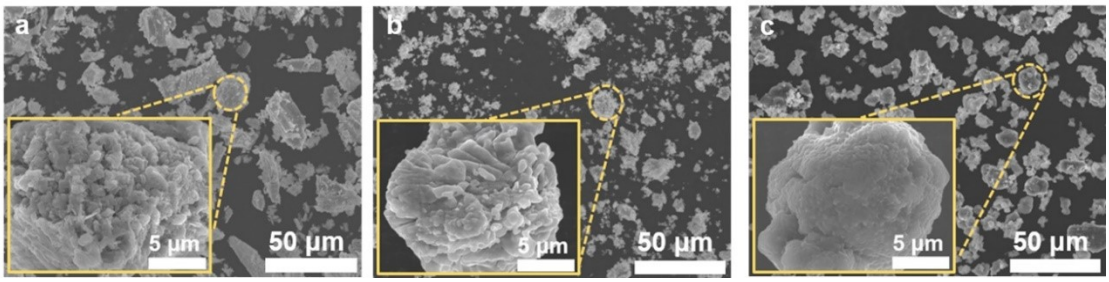

Figure S 5 SEM images of pristine powders: (a) Li_3InCl_6, (b) Ball-milled Li_3InCl_6, and (c) Li_6PS_5Cl.

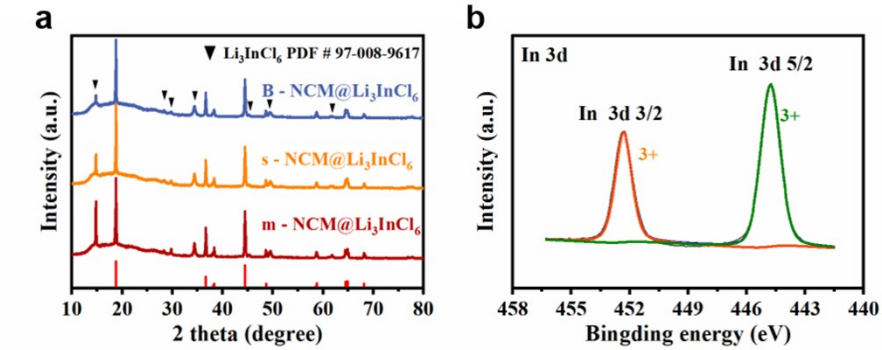

Figure S 6 (a) XRD of m-NCM@Li_3InCl_6, s-NCM@Li_3InCl_6, and B-NCM@Li_3InCl_6. (b) In 3d XPS spectra of pristine B-NCM@Li_3InCl_6.

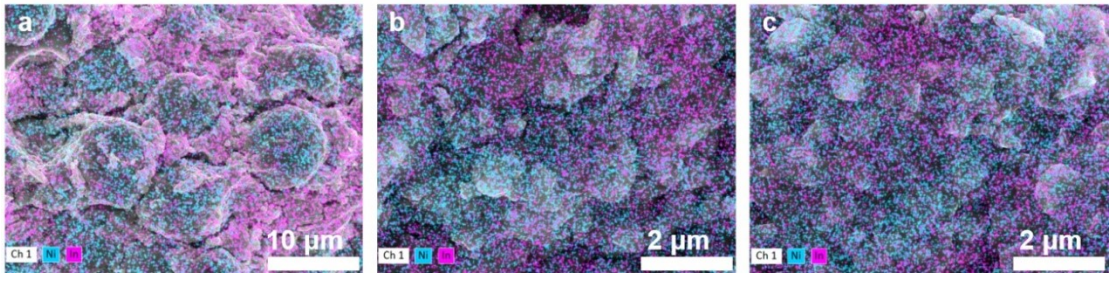

Figure S 7 EDS mappings for Ni and In elements of (a) m-NCM@Li_3InCl_6, (b) s-NCM@Li_3InCl_6 and (c) B-NCM@Li_3InCl_6.

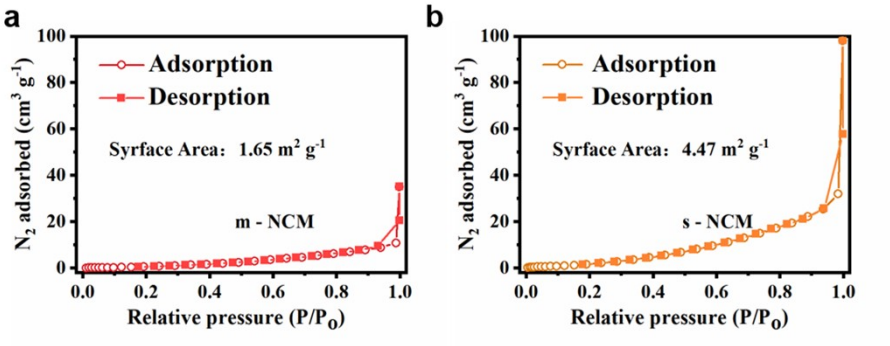

Figure S 8 BET dates of: (a) m-NCM and (b) s-NCM.

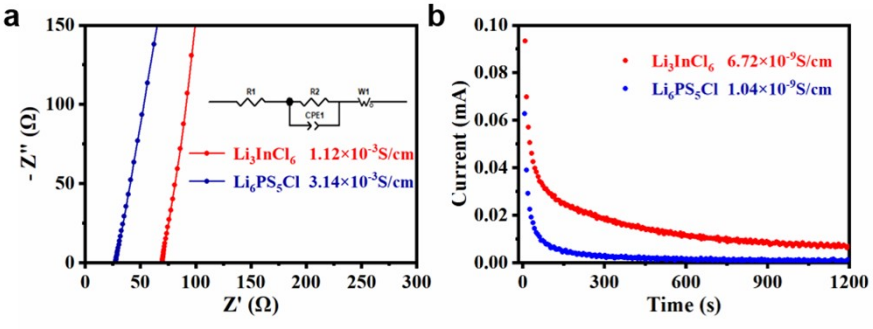

Figure S 9 (a) Alternating current (AC) and (b) DC polarization impedance results of ionic and electronic conductivities of Li_6PS_5Cl and Li_3InCl_6 at room temperature.

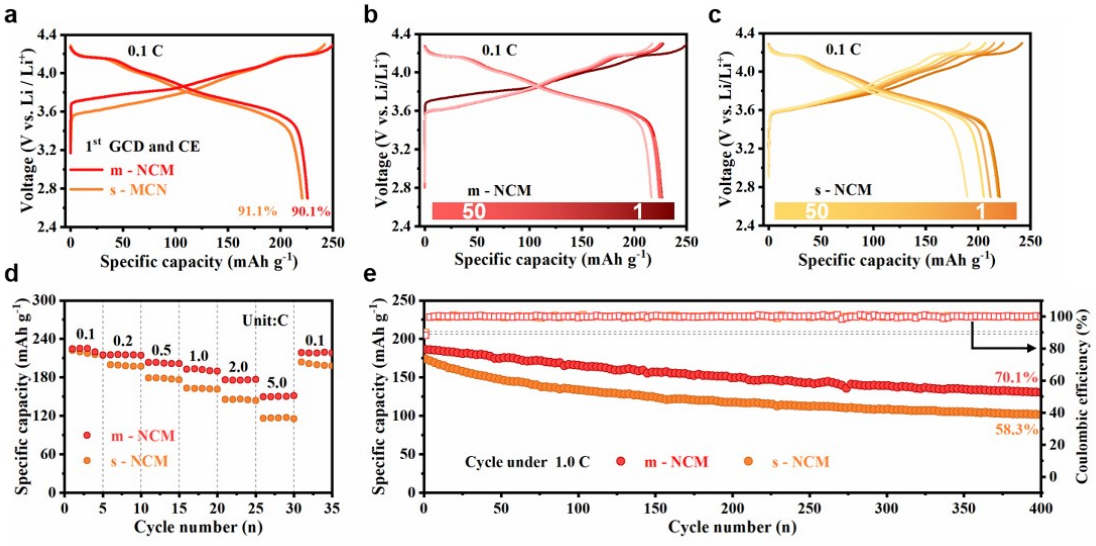

Figure S 10 Performance of Liquid-Electrolyte Batteries were based on m-NCM and s-NCM.

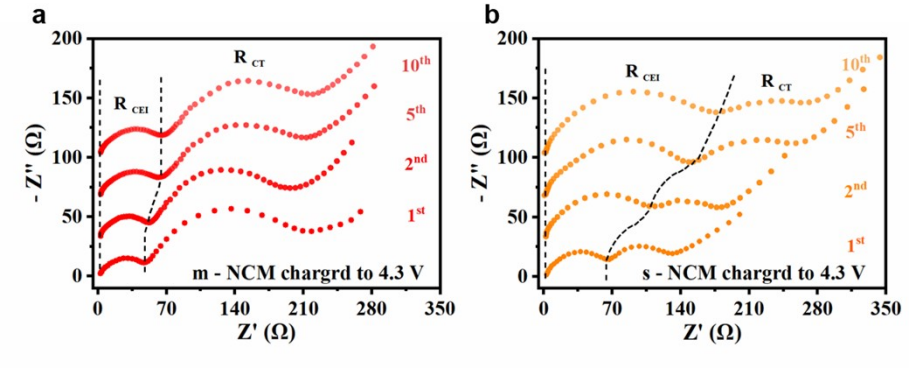

Figure S 11 The electrochemical impedance spectra of (a) m-NCM and (b) s-NCM in liquid batteries from the 1st to the 10th cycle.

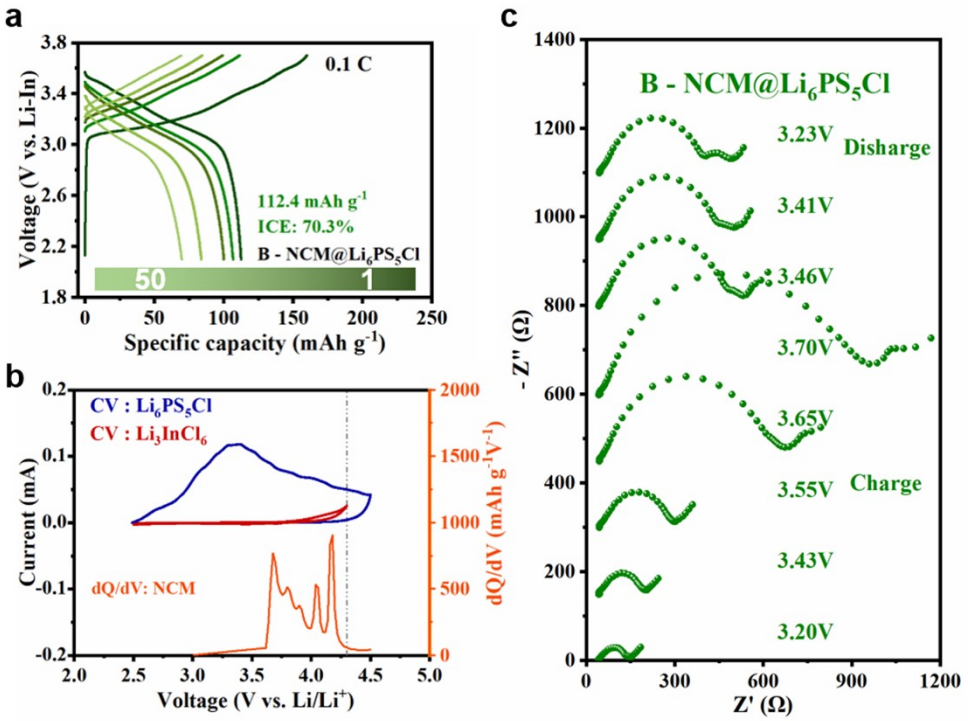

Figure S 12 (a) Galvanostatic charge-discharge profiles of B-NCM@ Li_6PS_5Cl cathode in ASSLBs at the voltage range of 2.1-3.7 V (*vs.* Li^+/Li-In) at 0.1C. (b) CV curves for Li_6PS_5Cl/C and Li_3InCl_6/C composites all-solid-state half-cells, and the first cycle dQ/dV plot for NCM half-cells with liquid electrolyte. (c) In-situ EIS spectra of B-NCM@ Li_6PS_5Cl cathode in ASSLBs recorded intermittently during galvanostatic batteries of first cycling at 0.1 C, 2.1-3.7 V (*vs.* Li^+/Li-In).

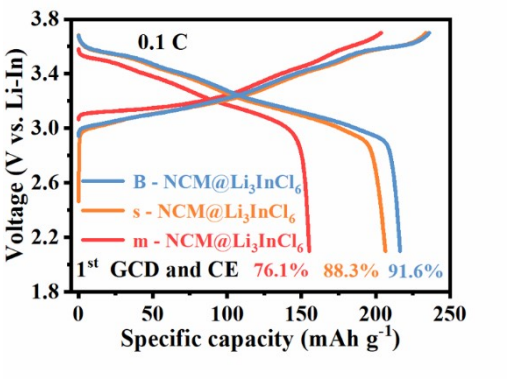

Figure S 13 First cycle of (a) m-NCM@Li_3InCl_6, (b) s-NCM@Li_3InCl_6 and (c) B-NCM@Li_3InCl_6 at 0.1C.

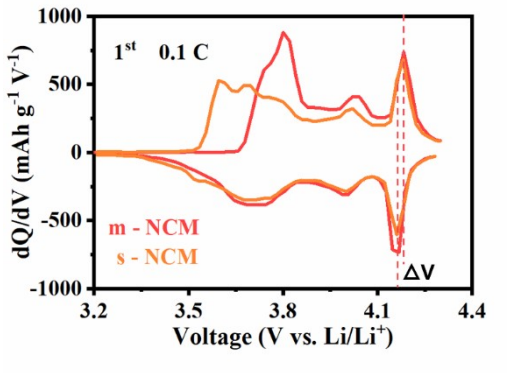

Figure S 14 dQ/dV of m-NCM and s-NCM in Liquid-Electrolyte batteries at the first cycle 0.1C.

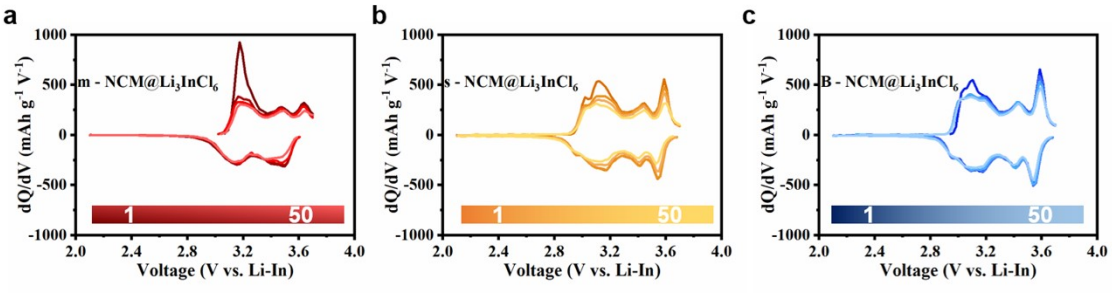

Figure S 15 dQ/dV of (a) m-NCM@Li_3InCl_6, (b) s-NCM@Li_3InCl_6 and (c) B-NCM@Li_3InCl_6 for 50 cycles at 0.1C.

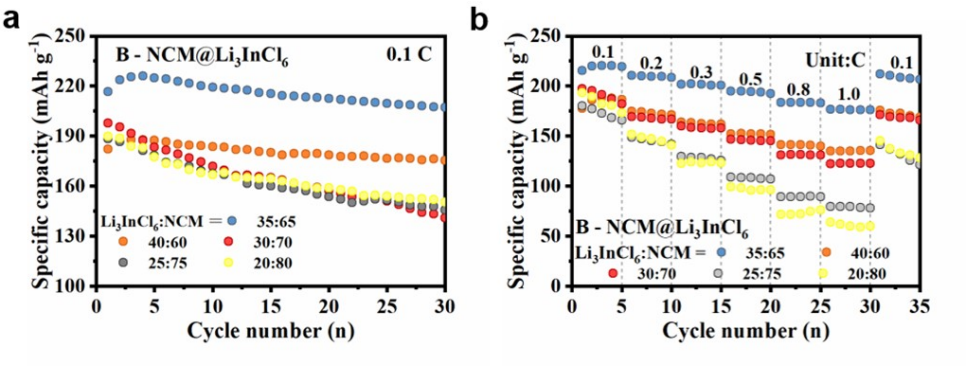

Figure S 16 Performance of B-NCM@Li_3InCl_6 with different mass ratios of Li_3InCl_6 and NCM.

As shown in Figure S16, the effect of cathode loading in B-NCM@ Li_3InCl_6 on electrochemical performance is investigated. The highest capacity of 216.4 mA h g^{-1} is achieved when the mass ratio of NCM is 65%. This mass ratio is much lower than the typical cathode loading of 80% in liquid cells, owing to the large solid electrolyte fraction required to ensure sufficient ionic diffusion pathways. Accordingly, the cycling performance is also improved by the increase of solid electrolyte, with capacity retentions of 71.6%, 96.0% and 96.2% for 30, 35 and 40% Li_3InCl_6 weight fractions, respectively (Figure S16a). This result is consistent with the previous report[2] and might be because that excessive Li_3InCl_6 could accommodate the chemo-mechanical volume change and lead to fewer voids in the composite cathodes. In addition, the rate capability of B-NCM@ Li_3InCl_6 with 65% NCM is also superior to the other cathode loadings as illustrated in Figure S16b, further confirming the formation of interpenetrating networks for ion diffusion and electron transport.

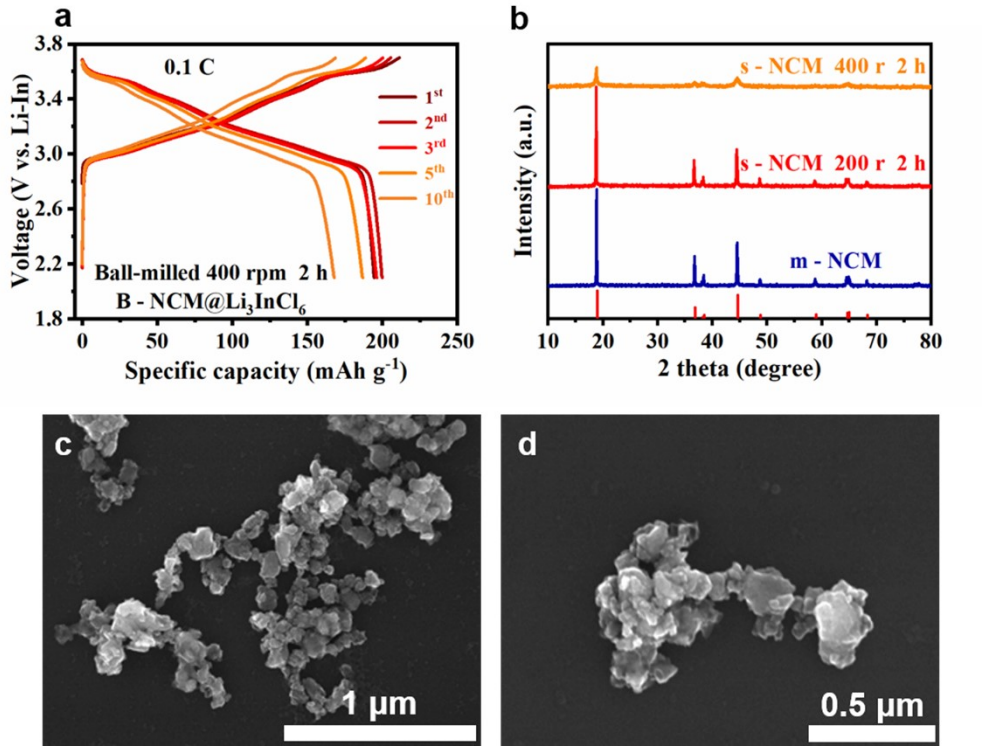

Figure S 17 (a) Performance of B-NCM@Li_3InCl_6 prepared by ball-milled for 400 rpm 2 h with mass ratios of LIC:NCM = 65:35. (b) XRD of pristine powders of m-NCM and s-NCM ball-milled by 400 rpm 2 h and 200rpm 2h. (c) and (d) SEM images of pristine powders of s-NCM ball-milled by 400 rpm 2 h.

The rapid decline in performance observed after ball-milling at 400 rpm can be attributed to the structural and microscopic degradation induced by high-energy forces. This phenomenon is illustrated in Figure S17 b, where the ball-milled NCM sample at 400 rpm exhibits partial amorphization with a significant decrease in reflection density. Additionally, the characteristic peak corresponding to the layered structure of NCM disappears at approximately 65°, indicating the destruction of this layered arrangement. Furthermore, Figure S17 c and d display that the particle size of the NCM sample milled at 400 rpm is notably smaller compared to that milled at 200 rpm, potentially leading to an increased number of interfaces and subsequent side reactions. Consequently, the electrochemical performance of NCM deteriorates, resulting in a substantial capacity loss of 18.1% after 10 cycles. (Figure S17a)

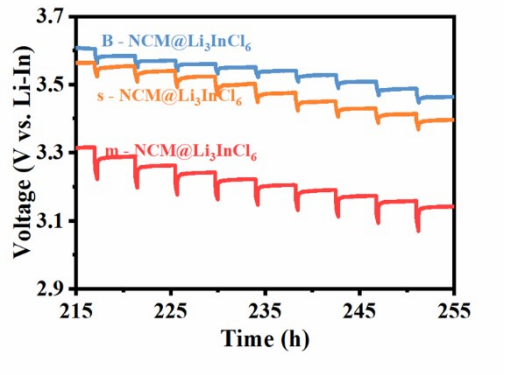

Figure S 18 Partial discharging process during the GITT test of m-NCM@Li_3InCl_6, s-NCM@Li_3InCl_6 and B-NCM@Li_3InCl_6.

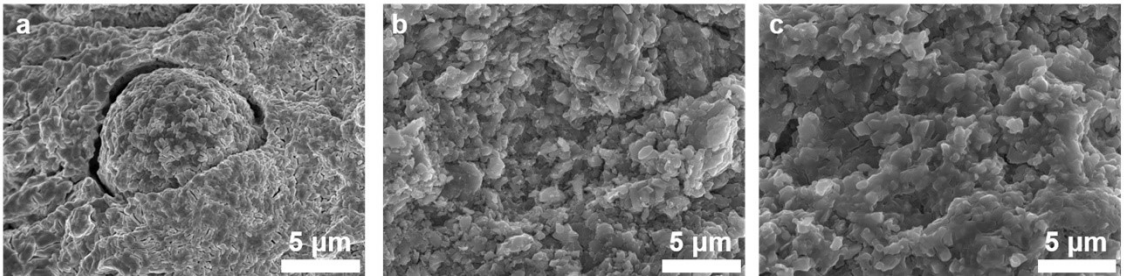

Figure S 19 SEM of (a) m-NCM@Li_3InCl_6, (b) s-NCM@Li_3InCl_6 and (c) B-NCM@Li_3InCl_6 after first charging process.

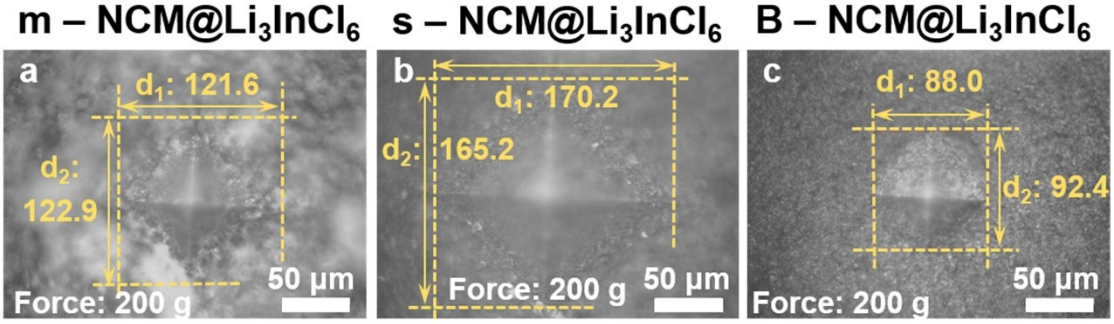

Figure S 20 The Vickers hardness test of (a) m-NCM@Li_3InCl_6, (b) s-NCM@Li_3InCl_6 and (c) B-NCM@Li_3InCl_6.

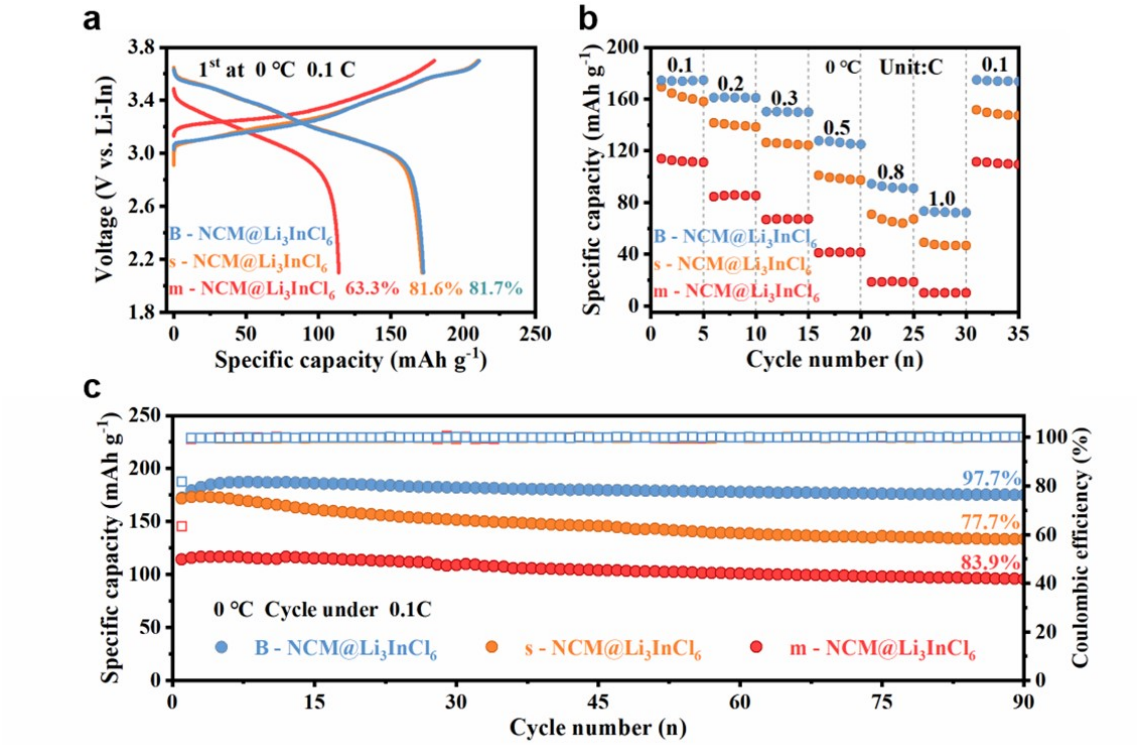

Figure S 21 (a) First cycle (b) rate performance and (c) Cycle performance of m-NCM@Li_3InCl_6, s-NCM@Li_3InCl_6 and B-NCM@Li_3InCl_6 composited cathodes at 0 ℃.

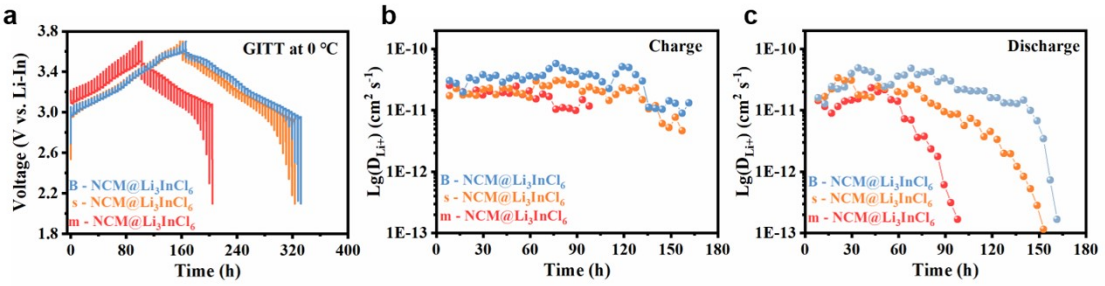

Figure S 22 (a) GITT test and D_{Li^+} of m-NCM@Li_3InCl_6, s-NCM@Li_3InCl_6 and B-NCM@Li_3InCl_6 at (b) charging and (c) discharging process at 0 ℃.

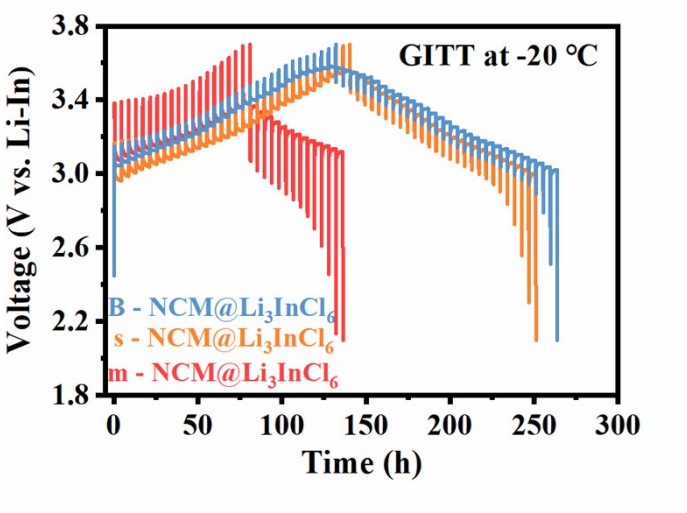

Figure S 23 GITT test of m-NCM@Li_3InCl_6, s-NCM@Li_3InCl_6 and B-NCM@Li_3InCl_6 at 0 °C.

	Li	Ni	Co	Mn
m-NCM	0.991	0.906	0.052	0.046
s-NCM	0.985	0.910	0.049	0.051

Table S 1 ICP-MS results of m-NCM and s-NCM.

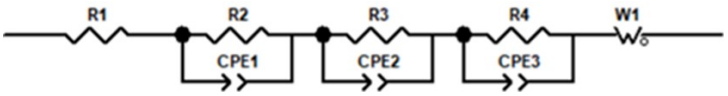

Point		Resistance (ohm)		
Cycle	Voltage (V)	R_{SE}	$R_{Cathode/SE}$	$R_{Anode/SE}$
1st	3.20	45.6	197.2	4.2
	3.43	46.0	160.2	3.8
	3.55	48.4	224.2	4.6
	3.65	49.2	453.6	28.6
	3.70	49.5	560.8	184.2
	3.46	50.5	262.7	59.2
	3.41	50.6	240.2	123.2
	3.23	51.4	210.5	142.1
2nd	3.20	53.3	212.3	59.2
50th	3.20	94.2	456.1	96.5

Table S 2 The fitting results of EIS spectra of ASSLBs with m-NCM@Li_3InCl_6 in Figure 3.

Point		Resistance (ohm)		
Cycle	Voltage (V)	R_{SE} (ohm)	$R_{Cathode/SE}$	$R_{Anode/SE}$
1st	3.20	37.1	18.3	6.0
	3.43	38.7	21.3	6.3
	3.55	38.9	33.7	6.2
	3.65	39.9	62.4	4.5
	3.70	40.3	107.2	6.9
	3.46	42.4	33.4	9.5
	3.41	45.2	28.9	23.7
	3.23	45.7	18.9	45.2
2nd	3.20	45.3	22.6	6.8
50th	3.20	57.7	182.5	41.6

Table S 3 The fitting results of EIS spectra of ASSLBs with s-NCM@Li_3InCl_6 in Figure 3.

Point		Resistance (ohm)		
Cycle	Voltage (V)	R_{SE} (ohm)	$R_{Cathode/SE}$	$R_{Aode/SE}$
1st	3.20	45.7	14.3	2.6
	3.43	46.4	15.2	2.7
	3.55	46.6	23.7	4.0
	3.65	48.2	35.2	5.2
	3.70	50.2	63.2	8.2
	3.46	50.8	16.2	9.2
	3.41	50.6	13.2	24.2
	3.23	50.5	14.9	38.0
2nd	3.20	50.1	15.2	11.0
50th	3.20	50.4	128.7	30.3

Table S 4 The fitting results of EIS spectra of ASSLBs with B-NCM@Li_3InCl_6 in Figure 3.

1. Y. Shang, Z. Liu, J. Dong, M. Yao, Z. Yang, Q. Li, C. Zhai, F. Shen, X. Hou, L. Wang, N. Zhang, W. Zhang, R. Fu, J. Ji, X. Zhang, H. Lin, Y. Fei, B. Sundqvist, W. Wang and B. Liu, Nature, 2021, **599**, 599-604.
2. Y. Han, S. H. Jung, H. Kwak, S. Jun, H. H. Kwak, J. H. Lee, S. T. Hong and Y. S. Jung, Adv. Energy Mater., 2021, **11**, 2100126.